WILEY

ARTICLE OPEN ACCESS

Engineering an Overflow-Responsive Regulation System for Balancing Cellular Redox and Optimizing Microbial Production

Jianli Zhang | Jian Wang | Tian Jiang | Xinyu Gong | Qi Gan | Yuxi Teng | Yusong Zou | Ainoor Anwar Dawadi | Yajun Yan 🔟

School of Chemical, Materials and Biomedical Engineering, College of Engineering, The University of Georgia, Athens, Georgia, USA

Correspondence: Yajun Yan (yajunyan@uga.edu)

ABSTRACT

Escherichia coli accumulates acetate as a byproduct in fast growth aerobic conditions when using glucose as carbon source. This phenomenon, known as overflow metabolism, has negative impacts on cell growth and protein expression, also causes carbon loss during biosynthesis in most microbial production scenarios. In this study, we regarded the "waste" metabolite as a useful metabolism indicator, constructed an overflow biosensor to monitor the change of acetate concentration and converted the signal into various regulation outputs. Phloroglucinol is a phenolic compound with several derivatives that exhibit various pharmacological activities. By applying the bifunctional dynamic regulation system on the phloroglucinol production, we released the cellular redox pressure in real-time and reduced the waste of carbon flux on overflow metabolism. Finally, carbon flux was redirected more favorably towards the desired product, resulting in a boosted phloroglucinol titer of 1.30 g/L, increased by 2.04-fold. Overall, this study explored the use of a central byproduct-responsive biosensor system on improving cellular metabolic status, providing a general approach for enhancing bioproduction.

1 | Introduction

Cells have evolved ingenious mechanisms to adapt to starvation, enabling survival and proliferation in extreme conditions (Gray et al. 2019; Parenteau et al. 2019). Similarly, when cells rapidly grow in a nutritious environment, the cellular metabolism is also subject to various regulations. Overflow metabolism is one prevalent strategy to cope with the fast consumption of carbon source and the limitations of respiration, even under aerobic circumstances (Vemuri et al. 2007). In the case of *Escherichia coli* (*E. coli*), rapid glucose uptake leads to a substantial accumulation of acetate as a result of elevated glycolysis (Harden 1901). Likewise, yeast cells exhibit

aerobic ethanol excretion, a phenomenon known as the "Crabtree effect" (Crabtree 1929), and mammalian cells, particularly cancer cells, exhibit lactate secretion, termed the "Warburg effect" (Warburg 1956). In the past few decades, researchers have devoted extensive efforts to unravel the mechanisms underlying acetate overflow. And an increasing amount of evidence suggests that acetate overflow is highly related to maintaining the cellular homeostasis under different growth conditions. Vemuri et al. reported the influence of the $NADH/NAD^+$ ratio on acetate overflow (Vemuri et al. 2006). Basan et al. demonstrated that the overflow mechanism is a programmed global response for balancing the changing proteomic demands (Basan et al. 2015).

Although acetate overflow has been proven to play a crucial role in the cellular metabolism regulation networks, the accumulated acetate is usually regarded as a detrimental metabolic waste in most microbial production scenarios. Acetate poses several adverse effects, such as impairing the cell growth and the expression of heterologous proteins (Jensen and Carlsen 1990; Koh et al. 1992; Nakano et al. 1997). Furthermore, the acetate pathway competes with the production pathways of acetyl-CoA downstream compounds, leading to a loss of carbon flux on metabolic byproducts (March et al. 2002). To address this issue, many approaches have been adopted to minimize the accumulation of acetate in microbial cell factories (MCFs). These include disrupting the acetate synthesis pathway (Bauer et al. 1990; Gecse et al. 2024), disrupting the glucose phosphotransferase system (PTS) (De Anda et al. 2006; Wong et al. 2008), diverting carbon flux to alternative product (Aristidou et al. 1995), expressing heterologous NADH oxidase and optimizing fermentation conditions (Vemuri et al. 2006). However, it has proven challenging to completely remove acetate from cells without compromising normal cell growth.

The net acetate accumulation results from the dynamic balance of the acetate synthesis pathway, which is determined by the changing metabolic states (Enjalbert et al. 2017; Millard et al. 2023). This makes it challenging to follow the real-time metabolic status by using conventional static methods, posing an obstacle to acetate removal. Specifically, when the glucose uptake rate reaches a certain threshold, it leads to an imbalance in the consumption and generation of acetyl-CoA, leading to the accumulation of acetate (Millard et al. 2021). According to previous research and hypotheses, acetate overflow serves as a strategy for cells to balance their redox ratio (Vemuri et al. 2006). The rapid influx of carbon flow into the tricarboxylic acid (TCA) cycle generates a substantial amount of NADH reducing power, exceeding the cell's oxidative capacity. Acetate pathway provides an alternative carbon flux outlet which can also generate energy through substrate-level phosphorylation without releasing any reducing power. Therefore, redirecting carbon flow into the acetate synthesis pathway helps alleviate the accumulation of reducing power and maintain cellular homeostasis.

Genetically encoded biosensor is a powerful tool capable of achieving dynamic regulation (Teng et al. 2022). As biosensors are commonly engineered based on transcriptional factors (TFs), they typically possess the ability to respond to specific metabolites or environmental factors and then transfer the signals into the transcription level of corresponding promoters (Teng et al. 2022). When applied in MCFs, biosensors are able to achieve the screening of high-yield producers, optimizing protein expression and dynamic regulating of synthetic pathways (d'Oelsnitz et al. 2022; Rogers and Church 2016). The effector type determines the application potential of a biosensor system. For instance, biosensors that respond to synthetic pathway intermediates or final products can be used to design pathway-specific regulation systems (Zhang et al. 2012), and quorum sensing biosensors can support biomass-dependent dynamic regulation (Gupta et al. 2017). Farmer and Liao developed an acetyl-phosphate (acetyl-P) biosensor based on the E. coli Ntr regulon. Acetyl-P has been considered as an indicator of glucose availability, and the biosensor was successfully utilized to improve the production of lycopene (Farmer and Liao 2000). However, using overflow waste as a biosensor effector remains an underexplored field.

The accumulation of acetate signifies a series of metabolic events: (1) rapid glucose uptake, (2) the generation rate of malonyl-CoA exceeding its consumption rate, and (3) excessive accumulation of NADH. Accordingly, in this study, we chose acetate as an ideal metabolic indicator. Firstly, we characterized an acetate-responsive biosensor, HpdR/P_{hpdH} variant. Subsequently, we established a bifunctional dynamic regulation system step by step to explore the potential of this biosensor in balancing the redox ratio, alleviating acetate overflow, and optimizing carbon flux distribution. Phloroglucinol is a value-added phenolic compound; many of its derivatives possess pharmacological activities such as antibacterial and anti-inflammatory activities (Khan et al. 2022; Kim and Kim 2010). The synthetic pathway of phloroglucinol was chosen as a proof of concept since the direct precursor of phloroglucinol is malonyl-CoA, and the amount of malonyl-CoA can reflect the potential of carbon flux from glycolysis entering into the production pathway through the acetyl-CoA node. We selected the regulation targets by focusing on NADH-related genes, and there were no pathway genes involved in the dynamic regulation circuits. Thus, potentially our dynamic regulation system could be a general platform for improving various acetyl-CoA downstream synthetic pathways. Finally, we validated that the increased production was accompanied by decreased acetate accumulation and decreased NADH/NAD$^+$ ratio, confirming the feasibility of using overflow metabolites as indicators to balance redox and improve carbon flux allocation. Overall, this study provides novel insights for understanding and exploring central metabolic pathway to enhance microbial-based production.

2 | Materials and Methods

2.1 | Experimental Materials

All strains used in this study are listed in Supporting Information S1: Table 1. Luria-Bertani (LB) medium containing 10 g/L tryptone, 10 g/L NaCl, and 5 g/L yeast extract was used for E. coli inoculation and plasmid propagation. M9Y medium containing 20 g/L glucose, 5 g/L yeast extract, 1 g/L NH$_4$Cl, 6 g/L Na$_2$HPO$_4$, 3 g/L KH$_2$PO$_4$, 0.5 g/L NaCl, 1 mM MgSO$_4$, and 0.1 mM CaCl$_2$ was used for phloroglucinol biosynthesis. 100 mg/L ampicillin and 50 mg/L kanamycin were added to the medium when necessary. IPTG was used for induction with a final concentration of 0.5 mM. The E. coli strain XL1-Blue (Stratagene, La Jolla, CA) was used for plasmids construction and storage. The E. coli strain BW25113(F') was used for the biosynthesis of phloroglucinol. BW25113(F') knockout derivatives were created via the P1 phage transduction method (Thomason et al. 2007). The dCas9 integrated strain employed in this study was previously constructed in our lab (Wang et al. 2023). Standard chemicals, including phloroglucinol, sodium acetate, sodium lactate, sodium formate, sodium citrate and disodium 2-oxoglutarate were purchased from Sigma-Aldrich (St Louis, MO, USA).

2.2 | DNA Manipulation

All DNA manipulations were conducted by following the standard molecular cloning protocols (Gibson et al. 2009). Quick ligation kit, Phusion high-fidelity DNA polymerase and restriction DNA endonucleases were purchased from New England Biolabs (Ipswich, MA, USA). Plasmids employed in this study are listed in Supporting Information S1: Table 1. The gene *phlD* (AAY95147.1) was amplified from *Pseudomonas protegens* Pf-5, the gene *noxE* (AAK04489.1) was amplified from *Lactococcus lactis* subsp. lactis. And genes *ndh* (946792), *cysJ* (947239), and *aroE* (947776) were amplified from *E. coli* genome. Plasmids pMK-MCS (Zou et al. 2024) and pHA-P_{LlacO1}-egfp (Li et al. 2023) were obtained from our previous studies. *Kpn*I and *Bam*HI were used to insert *phlD* into pMK-MCS to construct plasmid pMK-P_{LlacO1}-phlD. For characterizing the biosensor system, the biosensor plasmid pCS-$P_{lpp1.0}$-HpdR-P_{hpdH}-egfp was previously constructed in our lab (Wang et al. 2021). The biosensor control plasmid, pCS-$P_{lpp1.0}$-HpdR-P_{LlacO1}-egfp, was constructed by substituting P_{hpdH}-egfp with P_{LlacO1}-egfp with *Sal*I and *Bam*HI. The negative control plasmid for bioproduction, pMK-$P_{lpp1.0}$-HpdR-P_{LlacO1}-phlD, was constructed by inserting $P_{lpp1.0}$-HpdR into pMK-MCS with *Aat*II and *Bam*HI, then inserting P_{LlacO1}-phlD with *Xba*I and *Sac*I. To construct the dynamic repression plasmids, sgRNA variants were designed and constructed into a biosensor system using *Eco*RI and *Bam*HI, resulting in pCS-$P_{lpp1.0}$-HpdR-P_{hpdH}-sgRNAs. The corresponding static control plasmids pCS-$P_{lpp1.0}$-HpdR-P_{LlacO1}-sgRNAs were constructed based on the biosensor control plasmid by substituting egfp with sgRNAs. To introduce the phloroglucinol pathway gene, P_{LlacO1}-phlD was inserted using *Xba*I and *Sac*I, resulting in dynamic repression plasmids pCS-$P_{lpp1.0}$-HpdR-P_{hpdH}-sgRNAs-P_{LlacO1}-phlD and static control plasmids pCS-$P_{lpp1.0}$-HpdR-P_{LlacO}-sgRNAs-P_{LlacO1}-phlD. To construct the dynamic overexpression plasmids and the corresponding static control plasmids, the selected genes were amplified by PCR and inserted into the biosensor plasmid and negative control plasmids using *Eco*RI and *Bam*HI, resulting in pCS-$P_{lpp1.0}$-HpdR-P_{hpdH}-ndh/cysJ/aroE/noxE and pCS-$P_{lpp1.0}$-HpdR-P_{LlacO}-ndh/cysJ/aroE/noxE. P_{LlacO1}-phlD was inserted to introduce the phloroglucinol pathway, resulting in pCS-$P_{lpp1.0}$-HpdR-P_{hpdH}-ndh/cysJ/aroE/noxE-P_{LlacO1}-phlD and the static control plasmids pCS-$P_{lpp1.0}$-HpdR-P_{LlacO}-ndh/cysJ/aroE/noxE-P_{LlacO1}-phlD.

2.3 | Cultivation Conditions

For characterization of the HpdR/P_{hpdH}(V2) biosensor system, all transformants were randomly picked and inoculated into 3.5 mL fresh LB medium with appropriate antibiotics as seed culture. After overnight growing in a 37°C rotatory shaker at a speed of 270 rpm, 150 μL seed cultures were then transferred into fresh 3.5 mL fresh M9Y medium. Different concentrations of acetic acid, lactic acid, formic acid, citric acid, and 2-keto glutaric acid in sodium salt form were added initially, and the new cultures were cultivated in the 37°C rotatory shaker at a speed of 270 rpm. The samples were collected at the appropriate time point, and the cell density (OD_{600}) and green fluorescence intensities were measured.

For phloroglucinol biosynthesis. All transformants were inoculated into 3.5 mL LB medium with appropriate antibiotics and cultured in a 37°C rotatory shaker at a speed of 270 rpm for 8 h. Then, 2% (400 μL) seed cultures were transferred into 125 mL baffled flasks containing 20 mL M9Y and cultivated in a 30°C rotatory shaker at a speed of 270 rpm for 48 h. IPTG was added initially for induction with a final concentration of 0.5 mM. One milliliter cultures were sampled for the measurement of cell density (OD_{600}) and analyses of the products and metabolites by HPLC at the appropriate time point.

2.4 | Fluorescence Assays

Fluorescence was measured using the Synergy HT plate reader from Biotek. The samples were diluted by 10 times (20 μL sample with 180 μL DI water) and transferred into 96-well clear bottom plates (Corning 3603). The fluorescence intensity of eGFP was measured by using an excitation filter of 485/20 nm and an emission filter of 528/20 nm. Cell density (OD_{600}) was measured with the plate reader as well. The background signal from blank wells was subtracted. The eGFP fluorescence intensities were normalized with the corresponding cell densities to calculate the unit eGFP expression levels (eGFP/OD_{600}). All experiments were performed in triplicates, and the data are presented as the averages and standard deviations ($n = 3$).

2.5 | HPLC Analysis

The standard chemicals were dissolved with methanol or DI water. The HPLC samples were centrifuged at 12,000 rpm for 10 min. Phloroglucinol concentration was analyzed by Agilent HPLC 1260 Infinity II (1260 Infinity II Diode Array Detector WR) with a reverse-phase ZORBAX SB-C18 column. For phloroglucinol detection, methanol and 0.1% TFA were used as the mobile phase at a flow rate of 1 mL/min. The analyzing method was set as follows: 5% methanol from 0 to 10 min, 5%–10% methanol from 10 to 13 min, 10%–5% methanol from 13 to 15 min. Phloroglucinol can be detected at 4.8 min. Acetate and glucose were analyzed by Dionex Ultimate 3000 (Ultimate 3000 Photodiode Array Detector) with a Coregel-64H column (Transgenomic). 4 mM H_2SO_4 was used as the mobile phase at a flow rate of 0.4 mL/min for metabolite detection. The oven temperature was set to 45°C. Glucose and acetate can be detected at 16.3 min and 26.6 min respectively.

2.6 | Measurement of Intercellular NADH/NAD$^+$ Ratio

Intracellular concentrations of NADH and NAD$^+$ were detected by using the EnzyChrom NAD/NADH assay kit (BioAssay Systems, Hayward, CA, USA). The extraction and measurement were performed by following the manufacturer's protocol. Samples were centrifuged at 12,000 rpm for 10 min, and the cell pellets were harvested. The cells were washed with cold PBS and resuspended with acid extraction buffer (BioAssay Systems) or base extraction buffer (BioAssay Systems) for NAD$^+$ and NADH extraction, respectively. The NAD/NADH kit is based on

a lactate dehydrogenase cycling reaction. Specifically, NADH reduces a formazan reagent, generating a colored reduced product which can be measured at 565 nm (520–600 nm). The enzymatic reactions for the quantification of NADH and NAD^+ were conducted in flat-bottom 96-well clear bottom plates (Corning 3603).

2.7 | Statistics

For fluorescence assay and shake flask experiments, all data were reported as the mean ± standard deviation of biological triplicates ($n = 3$) and were presented in the figure legends. Data analysis was performed with Microsoft Excel. The colonies used for data collection were randomly selected from the agar plates.

3 | Results

3.1 | Acetate Overflow Is a Challenging Issue in Metabolic Engineering

During aerobic growth, cells primarily generate acetate originating from two major metabolic pathways: the Pta-AckA pathway and the PoxB-catalyzed pathway. The enzymes Pta and AckA catalyze two-step reversible reactions, converting acetyl-CoA into acetyl-phosphate and subsequently into acetate. The bidirectional pathway not only synthesises acetate but also facilitates the recycling and utilization of environmental acetate in the absence of other substrates (Figure 1a). Both pathways have been well studied as engineering targets to minimize acetate formation. However, strategies involving the elimination of these genes are compromised, potentially leading to additional problems (De Mey et al. 2007). When pta and/or ackA are knocked out, the reduction of acetate often coincides with a loss of cell growth and the accumulation of other metabolic by-products, such as lactate and formate (Contiero et al. 2000; Yang et al. 1999). Although lactate and formate are less toxic than acetate, they still result in carbon flux wastage. This suggests that cells may employ alternative pathways to balance metabolic pressure following disruption of the Pta-AckA pathway. PoxB contributes to aerobic growth of the cells, although non-essential, it has been shown to be crucial for cellular wellness (Abdel-Hamid et al. 2001). Despite knocking out poxB leading to an increase in pyruvate, the accumulation of acetate is not significantly reduced (Causey et al. 2004). Overall, blocking the acetate pathways cannot fundamentally solve acetate overflow.

To provide an ideal context for addressing acetate overflow, we chose the phloroglucinol synthetic pathway as a proof of concept. The production of phloroglucinol utilizes three malonyl-CoA molecules as direct precursors, catalyzed by the type III polyketide synthase, PhlD (Achkar et al. 2005; Zha et al. 2006). Previous studies have demonstrated that increasing the
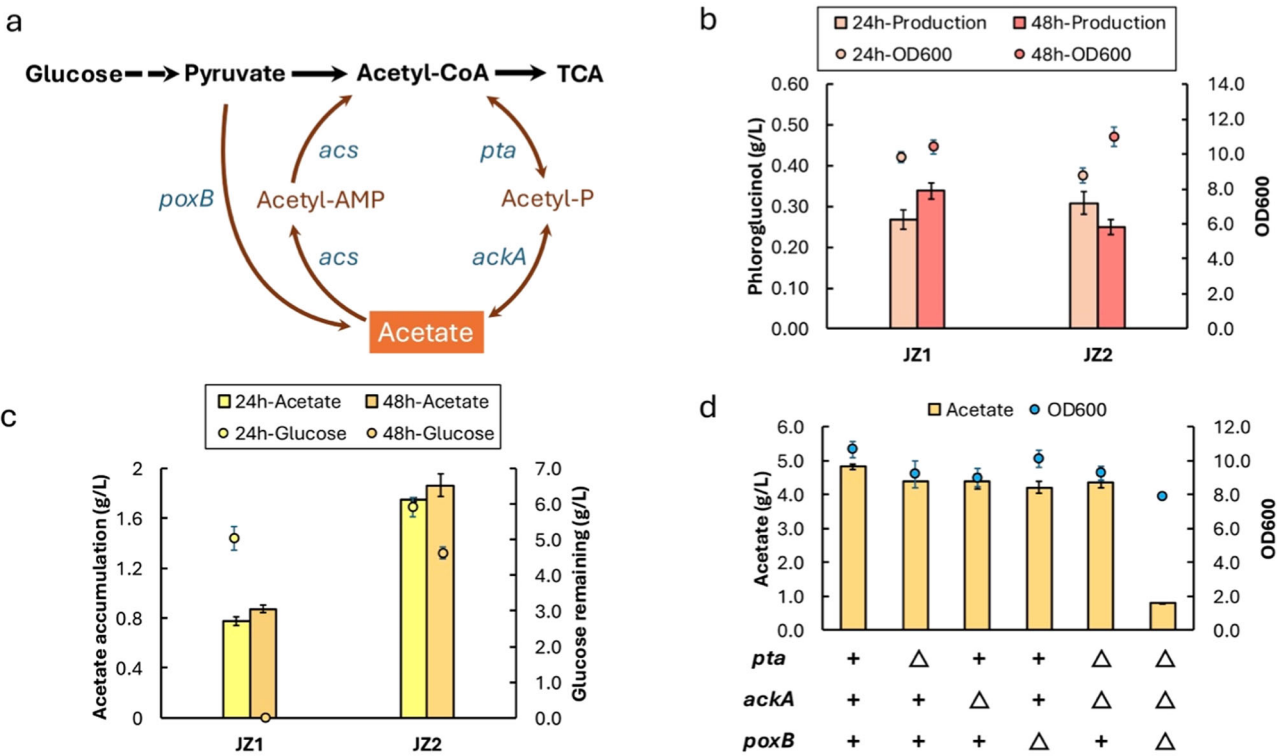
FIGURE 1 | Acetate overflow is a common and stubborn problem. (a) The schematic diagram of the synthesis pathways of acetate. pta, encodes phosphate acetyltransferase. ackA, encodes acetate kinase. acs, encodes acetyl-CoA synthetase. poxB, encodes pyruvate oxidase. Acetyl-P, acetyl phosphate. (b) The phloroglucinol production and cell growth of JZ1 strain (BW25113(F') with pMK-P$_{LlacO1}$-phlD) and JZ2 strain (BW25113(F') Δpta, ΔackA, ΔpoxB with pMK-P$_{LlacO1}$-phlD). (c) Acetate accumulation and the remaining glucose of JZ1 strain and JZ2 strain. (d) Acetate overflow level of different knockout strains. The data are reported as mean ± standard deviation from three biologically independent experiments ($n = 3$). The error bars represent standard deviation.

availability of acetyl-CoA can efficiently enhance phloroglucinol production (Yu et al. 2020). Therefore, by evaluating the titer of phloroglucinol, we can intuitively assess the amount of carbon flux directed towards desired products from the acetyl-CoA node. To construct the phloroglucinol synthetic pathway in *E. coli*, we cloned *phlD* gene from the genome of *Pseudomonas protegens* and integrated *phlD* into the medium copy plasmid pMK-MCS (Zou et al. 2024) to get pMK-P_{LlacO1}-phlD. By transferring the plasmid into WT *E. coli* strain BW25113(F'), we got the strain JZ1, which can produce 0.34 g/L phloroglucinol when growing in M9Y medium supplied with 20 g/L glucose as the carbon source (Figure 1b). Simultaneously, we identified 0.87 g/L acetate, indicating the presence of acetate overflow in the phloroglucinol production background (Figure 1c). To investigate the efficacy of knockout strategies within this specific pathway, we tried to isolate an acetate mutant with a minimized acetate level. By knocking out *pta*, *ackA*, *poxB* individually on WT, we got strains AC1, AC2, and AC3. Additionally, AC4 was created by knocking out both *pta* and *ackA*, and AC5 was created by knocking out *pta*, *ackA* and *poxB*. When cultivated in M9Y medium containing 20 g/L glucose, only strain AC5 exhibited a significant decrease in acetate production, whereas other strains maintained high acetate levels (Figure 1d). We then transferred pMK-P_{LlacO1}-phlD into AC5 to generate strain JZ2 for phloroglucinol production. However, to our surprise, the acetate level of JZ2 was even higher than JZ1, while the phloroglucinol production had no big difference between JZ2 and JZ1 (Figure 1b,c). This observation might be attributed to interference in cell metabolism. Furthermore, JZ2 remained 4.6 g/L glucose at 48 h of fermentation, while JZ1 completely consumed the glucose, indicating a slowdown in carbon source utilization due to the mutations (Figure 1c). Consequently, two pressing issues arose with the conventional knockout approach. Firstly, due to the complexity of the acetate overflow mechanisms, blocking the main acetate pathways may affect carbon flux distribution and may not effectively solve acetate accumulation or enhance the titer in some bioproduction scenarios. Secondly, acetate balance is a dynamic process, and relying on gene knockout as a constant regulation strategy may not be efficient enough and could adversely impact the wellness of cell metabolism.

In seeking an approach to fundamentally address acetate overflow and optimize carbon flux distribution, we started our work from understanding the mechanism of acetate overflow. In the metabolic network, NAD serves as a cofactor in over 300 reactions, and the NADH/NAD$^+$ ratio plays an essential role in regulating the transcription of numerous genes and the metabolic flux of various pathways (Holm et al. 2010; Vadali 2004). Previous studies have shown that a high NADH/NAD$^+$ ratio triggered acetate overflow, while expressing NADH oxidase completely eliminated acetate formation (Vemuri et al. 2006). In *E. coli*, NADH is predominantly generated through glycolysis and the TCA cycle. Rapid glycolysis leads to elevated NADH level and increased acetyl-CoA flux. Given that one turn of the TCA cycle can yield eight NAD(P)H and 2 FADH$_2$, while the acetate pathway does not generate any reducing power, diverting carbon flux from the acetyl-CoA node to acetate is considered a strategy for regulating redox homeostasis (Eiteman and Altman 2006). Inspired by this, we aim to mitigate acetate overflow by modulating the NADH/NAD$^+$ ratio, thereby establishing an optimal redox environment through an artificial regulation network.

3.2 | Characterizing an Acetate-Responsive Biosensor System

We attempted to seek a tool capable of tracking the dynamic fluctuations in acetate concentration. The TFs-based biosensor was opted because a properly engineered biosensor has the ability to monitor specific molecular concentrations in real-time and generate varying transcriptional strength as the outputs. *Pp*HpdR/P_{hpdH} is a 3-hydroxypropionic acid (3-HP)-inducible system identified and characterized from *Pseudomonas putida* (Hanko et al. 2017). As a LysR-type transcriptional regulator, HpdR binds upstream of the corresponding promoter P_{hpdH}, when the effector 3-HP interacts with HpdR, the transcription of P_{hpdH} will be activated (Maddocks and Oyston 2008) (Figure 2a). Due to the substrate promiscuity of *Pp*HpdR/P_{hpdH} system, it has also been engineered as biosensors for 3-hydroxybutryate (3-HB) and butyrate (Wang et al. 2023; Wang et al. 2021). Given the structural similarity between acetate and 3-HP/butyrate, we hypothesized that this system might have the potential to respond to acetate. To verify this hypothesis, we employed the HpdR/P_{hpdH} V2 variant, previously constructed in our lab on a medium copy plasmid. Through the truncation of a palindromic sequence upstream of P_{hpdH} and utilizing $P_{lpp1.0}$ promoter to control HpdR, the V2 variant was engineered to achieve a broader dynamic range (Wang et al. 2021). After transferring the V2 plasmid pCS-$P_{lpp1.0}$-HpdR-P_{hpdH}-egfp into BW25113(F') strain, we assessed the responsiveness and substrate specificity of the V2 system by supplying acetate and various other organic acids. The results indicated that V2 exhibited increased fluorescence in response to rising concentrations of acetate while showing no discernible response to other metabolites (Figure 2b). Subsequently, we tested the range of acetate concentrations to which the biosensor could respond by adding gradient acetate into the medium. Based on the response curve characterized using eGFP fluorescence, we identified a wide operational range of the V2 system from 0 to 10 g/L acetate, while the fluorescence intensity increased by 34.2-fold. (Figure 2c). Considering that the concentration of endogenous acetate usually does not reach pretty high levels, we further narrowed down the range of acetate concentration to 0–5 g/L to test the sensitivity and applicability of V2 system. The results showed that fluorescence intensity increased by 11.2-fold, indicating that V2 system has precise responsiveness to low acetate concentrations (Figure 2d). Due to the favorable response profile of V2 to acetate, we intended to utilize this system in subsequent experiments for monitoring acetate accumulation and supporting the construction of artificial dynamic regulation networks.

3.3 | Engineering Acetate-Responsive Dynamic Repression Circuits for Relieving Acetate Overflow and Enhancing Production

Considering the crucial role of acetate in redox balance, we speculated that establishing an artificial redox regulation
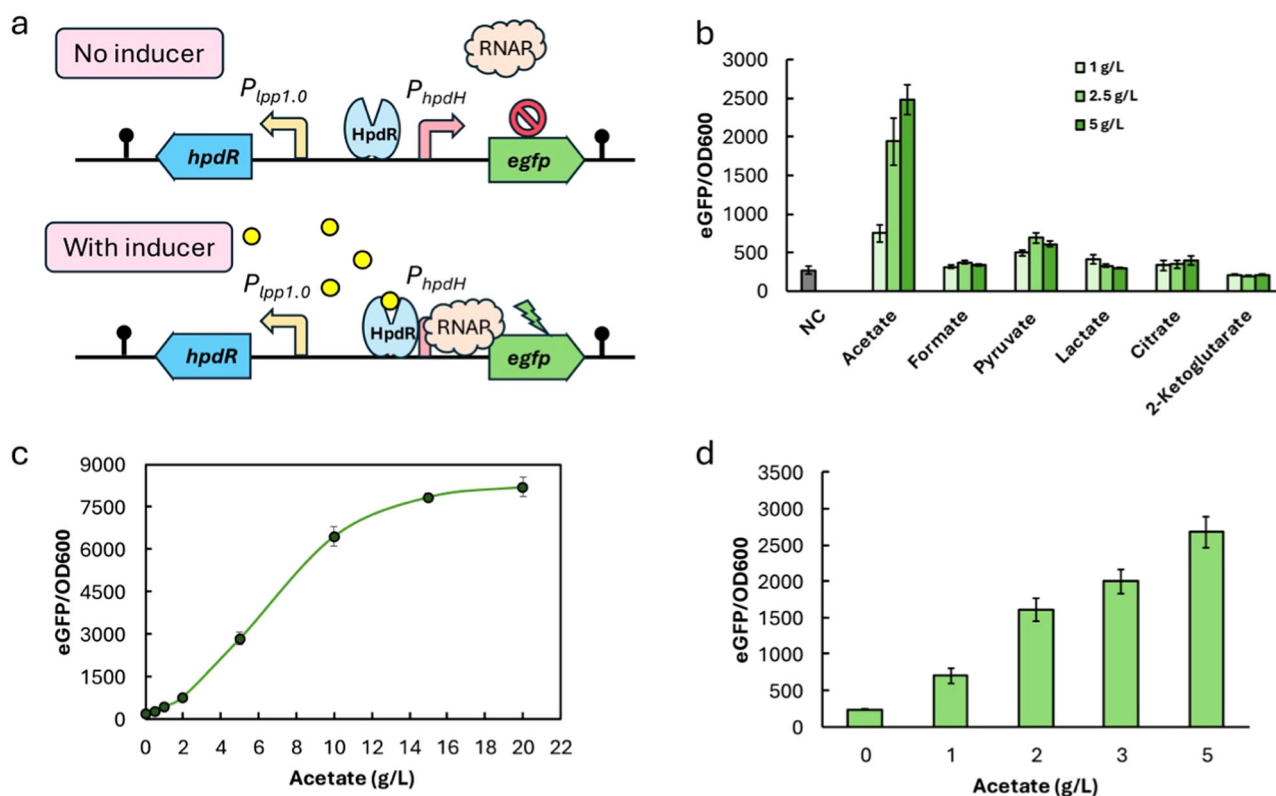
FIGURE 2 | Characterization of acetate responsive biosensor system. (a) The molecular mechanism of HpdR/P$_{hpdH}$ biosensor system. The yellow circles represent inducers. (b) Exploring the substrate specificity of HpdR/P$_{hpdH}$ (V2). NC indicates the negative control group, where no additional chemicals were fed. (c) The responsive curve of HpdR/P$_{hpdH}$ (V2) with adding gradient concentrations of sodium acetate. (d) The responsiveness of HpdR/P$_{hpdH}$ (V2) in a smaller operational range. The data are reported as mean ± standard deviation from three biologically independent experiments ($n = 3$). The error bars represent standard deviation.

system overlaid on the cell's intrinsic regulation to precisely inhibiting reducing power generation when the cell experiences reducing power surplus, can efficiently relieve the redox pressure. In this way, the cell would reduce the carbon flux used to alleviate redox pressure through the acetate pathway, decrease the waste of carbon flux from glycolysis source, and divert more carbon flux towards the acetyl-CoA downstream products, such as phloroglucinol. To achieve this regulatory effect, we aimed to build an artificial repression circuit using the HpdR/P$_{hpdH}$ V2 biosensor as a tool, with the accumulated acetate serving as an indicator. Specifically, in the initial stage of fermentation, when the glucose uptake rate is below the threshold for acetate overflow, acetate does not accumulate. During this period, the majority of carbon flux is directed towards cell growth, and the regulatory circuit remains inactive, ensuring a stable metabolism status. When glucose consumption accelerates, rapid generation of reducing power occurs via high-speed TCA cycle and glycolysis. To alleviate this reducing pressure, cells begin to divert carbon flux towards acetate production, thereby triggering acetate overflow. At this point, we expected acetate to serve as an effector, interacting with HpdR and then triggering P$_{hpdH}$-controlled repression of genes involved in NAD(P)H generation within the TCA cycle. In this way, the reducing stress would get alleviated within the TCA cycle without disrupting glycolysis flux. Moreover, the acetate pathway would become a less-preferred shunt, allowing more efficient utilization of the carbon source for the malonyl-CoA shunt (Figure 3).

By focusing on genes encoding enzymes involved in NAD(P)H generation within TCA cycle, we selected *icd*, *sucA*, *sucB* and *mdh*, we also included the two malate dehydrogenases genes *maeA* and *maeB*. In our selections, despite *icd* and *maeB* producing NADPH instead of NADH, we still tried to explore the repression effect of these genes as there are pathways for the interconversion between NAD and NADP. To implement the dynamic repression, we adopted the CRISPR interference (CRISPRi) system (Figure 4a). The BW25113(F') strain with the integration of P$_{LlacO1}$-dCas9 in the genome was employed in this study (Wang et al. 2021). Before proceeding the dynamic repression-aided production, we first validated the rationality of our design by conducting experiments to check if the V2-controlled CRISPRi can inhibit fluorescence protein expression based on acetate concentration. The sgRNA spacer sequence targeting on *egfp* was inserted into the biosensor plasmid, yielding pCS-P$_{lpp1.0}$-HpdR-P$_{hpdH}$-sgegfp. Additionally, a static regulation control was constructed by substituting P$_{hpdH}$ with the inducible promoter P$_{LlacO1}$ which has comparable strength (Supporting Information S1: Figure 1), yielding pCS-P$_{lpp1.0}$-HpdR-P$_{LlacO1}$-sgegfp. Both plasmids were individually co-transferred with pHA-P$_{LlacO1}$-egfp (Li et al. 2023) into the dCas9 integrated strain. Fluorescence measurements were taken upon the addition of gradient acetate from 0 to 5 g/L, resulting in a gradually decreasing of normalized fluorescence intensity from 4016 to 2092 for the dynamic group, validating the functionality of the dynamic repression circuits (Figure 4b). Then, we planned to apply this dynamic repression system to control the
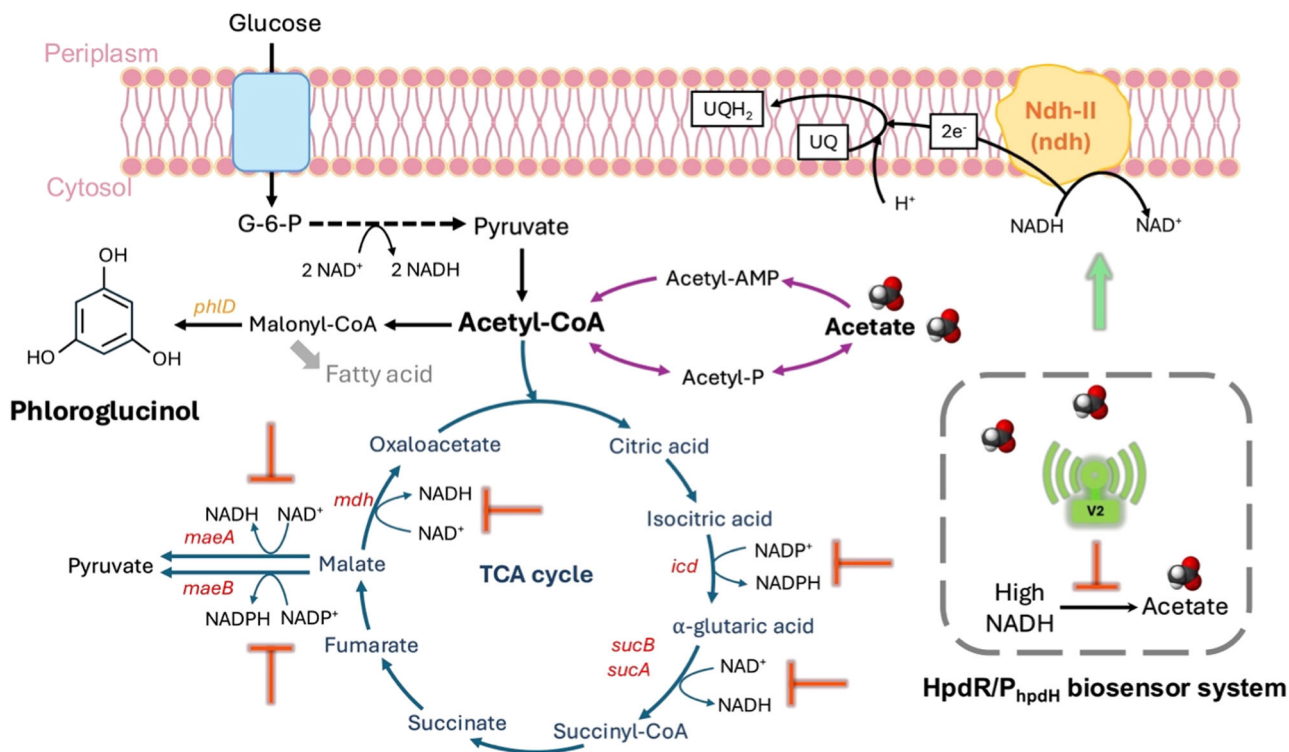
FIGURE 3 | Schematic representation of the dynamic regulation circuits of phloroglucinol pathway. The red inhibition arcs represent inhibition from the biosensor system, the green arrows represent overexpression from the biosensor system. Ndh-II, NADH:quinone oxidoreductase II. UQ, ubiquinones. UQH$_2$, ubiquinol. G-6-P, glucose-6-phosphate. *phlD*, encodes phloroglucinol synthase. *maeA*, encodes NAD$^+$-dependent malate dehydrogenase. *maeB*, encodes NADP$^+$-dependent malate dehydrogenase. *icd*, encodes isocitrate dehydrogenase. *sucA*, encodes 2-oxoglutarate decarboxylase. *sucB*, encodes 2-oxoglutarate dehydrogenase E2 subunit. *mdh*, encodes malate dehydrogenase.

selected genes and construct reducing power dynamic repression circuits. So, we designed different sgRNA spacers targeting the start codons of selected genes to replaced *sgegfp* in the above plasmids, yielding the dynamic repression plasmids pCS-P$_{lpp1.0}$-HpdR-P$_{hpdH}$-sgRNA(s) and the static regulation controls pCS-P$_{lpp1.0}$-HpdR-P$_{LlacO1}$-sgRNA(s). We also constructed plasmid pCS-P$_{lpp1.0}$-HpdR as the negative control.

Next, we tried to integrate the phloroglucinol pathway with the dynamic repression circuit and study whether this circuit can achieve the goal of alleviating acetate overflow and improve carbon flux reallocation in a plug-and-play manner for a specific pathway. So, we introduced the phloroglucinol pathway gene *phlD* under the control of P$_{LlacO1}$ into each of the aforementioned plasmids. This allowed us to detect the malonyl-CoA shunt by measuring the phloroglucinol production. Cells transformed with these plasmids were cultured in M9Y medium supplemented with 20 g/L glucose. After 48 h of fermentation, most strains with dynamic circuits, except to strain with inhibited *sucA*, exhibited increased production compared to the negative control and their corresponding static repression groups. Specifically, the groups with sg*maeA*, sg*maeB*, sg*icd*, sg*sucB* and sg*mdh* yielded 0.74, 0.74, 0.65, 0.61, and 0.78 g/L phloroglucinol, representing increases by 1.38-, 1.36-, 1.21-, 1.13- and 1.44-folds respectively when comparing with negative control, which produced 0.54 g/L phloroglucinol (Figure 4c). As expected, all dynamic repression groups had decreased acetate accumulation levels. Specifically, strains with sg*maeA*, sg*maeB*, sg*icd*, sg*sucA*, sg*sucB*, and sg*mdh* accumulated 0.73, 1.05, 0.34,

0.93, 0.51, and 0.52 g/L acetate, representing 0.49-, 0.70-, 0.22-, 0.62-, 0.34- and 0.35-fold of the acetate of negative control, demonstrating the relieving of acetate overflow and increased malonyl-CoA shunt (Figure 4d). However, except to the strain with static inhibited *mdh*, which produced 0.61 g/L phloroglucinol, most static control groups showed decreased titer (Figure 4c). This is possibly due to the constant repression on the central pathways disrupting normal metabolism, even from the beginning of fermentation. We further measured the NADH/NAD$^+$ ratio of all dynamic repression groups; the strains with sg*maeB* and sg*icd* showed decreased NADH/NAD$^+$ (Supporting Information S1: Figure 2). These results also confirmed the rationality of using acetate as an indicator to guide the timing of regulatory implementation, as well as the feasibility of using this dynamic repression circuit to relieve acetate overflow and conserve carbon flux to increase phloroglucinol production.

3.4 | Engineering Acetate-Responsive Dynamic Overexpression Circuits for Relieving Acetate Overflow and Improving Production

In contrast to the previous strategy of dynamically repressing reducing force production, we next sought enzymes that could be overexpressed to consume excess NADH. However, constantly overexpressing NADH-consuming enzymes would continuously decrease reducing power, disrupting the cellular redox balance. Therefore, we hypothesized that dynamically
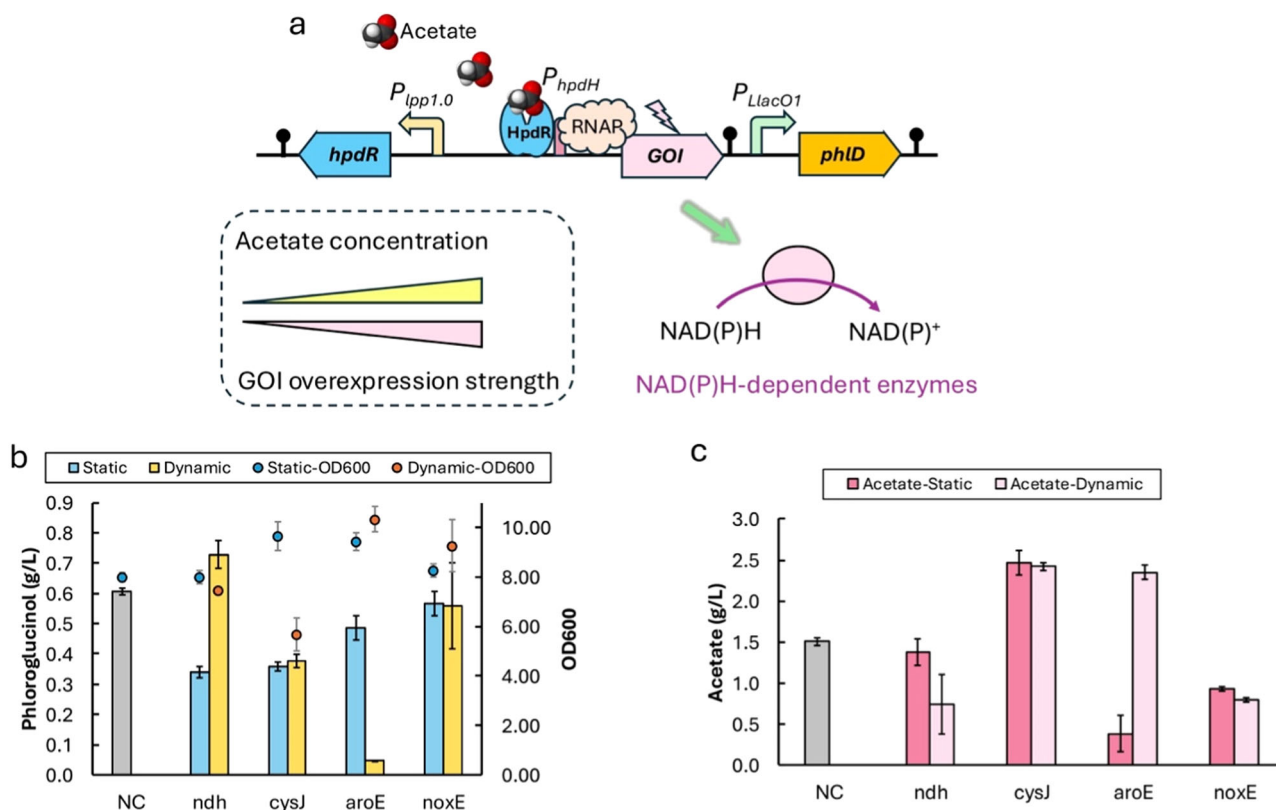
FIGURE 4 | The performance of the dynamic repression circuits. (a) The design and mechanism of the dynamic repression circuits. (b) The repression performance when statically or dynamically expressing *sgegfp* to inhibit *egfp* genes which on high copy plasmids. (c) The phloroglucinol production titer and cell growth when statically or dynamically inhibiting different target genes. (d) The accumulation of acetate when statically or dynamically inhibiting different target genes. NC indicates the phloroglucinol production strain harboring plasmid pCS-P$_{lpp1.0}$-HpdR-P$_{LlacO1}$-phlD. The data are reported as mean ± standard deviation from three biologically independent experiments ($n = 3$). The error bars represent standard deviation.

overexpressing these proteins only when NADH level exceeds the preferred threshold would be a more effective strategy (Figure 3). To figure out suitable NADH-dependent enzymes, we selected multiple candidates from different reaction categories. One such candidate is NADH:quinone oxidoreductase II (NDH-2), which is one of the two major NADH dehydrogenases in the *E. coli* respiratory chain. NDH-2 transfers electrons from NADH to the quinone pool, while another NADH dehydrogenase, NDH-1, contributes to both electron transfer and electrochemical gradient generation. Previous studies have suggested that NDH-2 is preferentially utilized in aerobic respiration (Tran et al. 1997). And strain lacking NDH-2 has exhibited a significant reduction in electron transfer from NADH, whereas strain lacking NDH-1 was only slightly affected (Liu et al. 2019; Tran et al. 1997). Hence, NDH-2 was chosen as a candidate enzyme for our study. We also selected *noxE*, which encodes a water-forming heterologous NADH oxidase from *Lactococcus lactis*, known for its ability to reduce intercellular NADH levels (Heux et al. 2006; Zhang et al. 2012). Furthermore, considering the presence of pathways for interconversion between NAD and NADP, we also included several NADPH-dependent enzymes-encoding genes in our selection, such as *cysJ*, which encodes the α subunit of sulfite reductase, and *aroE*, which encodes shikimate dehydrogenase.

To apply the dynamic overexpression design for consuming NADH, increasing acetyl-CoA flux and decreasing acetate overflow, we constructed a series of dynamic regulation plasmids by integrating HpdR regulator with the target genes under

the control of P$_{hpdH}$, yielding pCS-P$_{lpp1.0}$-HpdR-P$_{hpdH}$-ndh, pCS-P$_{lpp1.0}$-HpdR-P$_{hpdH}$-noxE, pCS-P$_{lpp1.0}$-HpdR-P$_{hpdH}$-cysJ and pCS-P$_{lpp1.0}$-HpdR-P$_{hpdH}$-aroE. Thus, the target genes were expected to have a dynamic overexpression pattern subject to the acetate accumulation (Figure 5a). To establish the static control for every target, we substituted the P$_{hpdH}$ promoter in the dynamic overexpression plasmids with the inducible promoter P$_{LlacO1}$, resulting in pCS-P$_{lpp1.0}$-HpdR-P$_{LlacO1}$-GOI. Thus, the target genes could be constantly overexpressed when adding IPTG. We also utilized the previous plasmid, pCS-P$_{lpp1.0}$-HpdR as the negative control. Furthermore, to confirm the effect of the plug-and-play dynamic overexpression circuit in acetyl-CoA downstream production, the P$_{LlacO1}$ controlled *phlD* was integrated into every plasmid for observing the carbon flux redistribution. After individually transferring these plasmids into the dCas9 integrated strain, we noticed that only strain harboring dynamic overexpressed *ndh* showed significantly elevated phloroglucinol production of 0.73 g/L, representing a 1.20-fold increase compared to the negative control (Figure 5b). This increase was accompanied by a decrease in acetate accumulation, which was 0.49-fold compared to the negative control and 0.54-fold compared to the static control (Figure 5c). However, the groups with other targets did not achieve improved production. Perhaps the overexpression of other enzymes causes an extra burden to the cell growth or cellular metabolism. Furthermore, we measured the NADH/NAD$^+$ ratio of the dynamic overexpression groups, only strain with dynamically overexpressed *ndh* showed decreased NADH/NAD$^+$ ratio (Supporting Information S1: Figure 2). Overall, the *ndh*

FIGURE 5 | The performance of the dynamic overexpression circuits. (a) The design and mechanism of the dynamic overexpression circuits. GOI, gene of interest. (b) The phloroglucinol production titer and cell growth when overexpressing different target genes. (c) The accumulation of acetate when overexpressing different target genes. NC indicates the phloroglucinol production strain harboring plasmid pCS-$P_{lpp1.0}$-HpdR-P_{LlacO1}-phlD. The data are reported as mean $\pm$ standard deviation from three biologically independent experiments ($n = 3$). The error bars represent standard deviation.

dynamic overexpression circuit proved to be an effective tool for increasing the malonyl-CoA shunt and was selected for further engineering.

3.5 | Establishing the Acetate-Responsive Bifunctional Circuits for Balancing the NADH/NAD$^+$ Ratio and Enhancing Production

To further explore optimal regulatory outcomes, we devised a plan to combine the well-performing repression and overexpression regulation targets to build bifunctional dynamic regulation circuits (Figure 6a). In this way, we expected to establish a bifunctional regulation logic: when acetate accumulates, the circuits would slow down the generation of reducing power in the central metabolic pathway, while simultaneously consuming the existing reducing power to reach a NADH/NAD$^+$ ratio favorable for the production of acetyl-CoA downstream compounds. We individually combined the *ndh* dynamic overexpression operon with four selected dynamic repression operons targeting *maeA*, *maeB*, *icd* and *mdh* to create four dynamic circuit plasmids pCS-$P_{lpp1.0}$-HpdR-P_{hpdH}-*ndh*-P_{hpdH}-sgRNA(s), we also constructed the static controls by employing P_{LlacO1} to obtain pCS-$P_{lpp1.0}$-HpdR-P_{LlacO1}-ndh-P_{LlacO1}-sgRNA(s). P_{LlacO1}-*phlD* was then integrated into these plasmids for phloroglucinol production. Upon transferring the bifunctional circuits into the dCas9 integrated strain, the strain harboring the combination of dynamically regulated *ndh* and sg*maeB* reached to the

highest production up to 1.30 g/L, which is 2.04-fold compared to the negative control (Figure 6b). Additionally, the strain harboring the combination of dynamically regulated *ndh* and *sgicd* also showed promising performance, reaching to 1.15 g/L phloroglucinol, representing an increase by 1.80-fold compared to the negative control (Figure 6b). Both bifunctionally regulated strains exhibited higher titer than their dynamic repression or dynamic overexpression counterparts. Besides, the two bifunctional regulated strains with sg*maeB* and sg*icd* accumulated 0.15 and 0.20 g/L acetate, showing decreases by 0.19-fold and 0.25-fold, respectively (Figure 6c). Based on these results, we proposed that by employing bifunctional dynamic regulation, we efficiently tuned the intracellular NADH/NAD$^+$ ratio to a level suitable for phloroglucinol production. Simultaneously, cells are less inclined to choose the acetate pathway to alleviate redox pressure, thereby diverting more carbon flux towards malonyl-CoA and ultimately increasing the production of phloroglucinol.

To further validate our hypothesis, we attempted to monitor the cellular redox levels of the two selected bifunctional combinations during the fermentation process. According to the results of time course fermentation (Supporting Information S1: Figure 3), we chose the 24-h and 36-h time points as representative stages. At 24-h, which marks the early phase of fermentation, phloroglucinol just starts to accumulate and acetate reaches the maximum concentration. The bifunctional regulation circuit is activated at its maximum strength. At 36-h, representing the late phase of
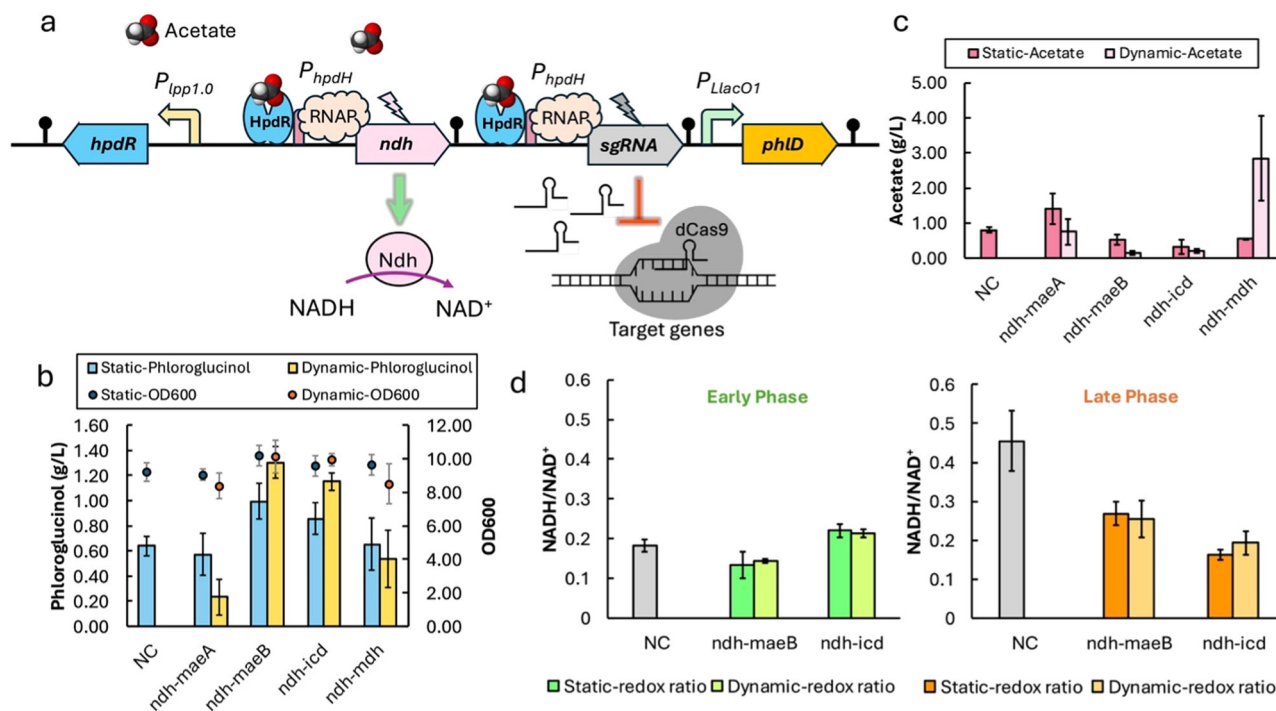
FIGURE 6 | The performance of the bifunctional dynamic regulation circuits. (a) The design and mechanism of the bifunctional dynamic regulation circuits. (b) The phloroglucinol production titer and cell growth when applying different regulation combinations. (c) The accumulation of acetate when applying different regulation combinations. (d) The NADH/NAD$^+$ ratio of selected combinations during the early phase and late phase of fermentation. Samples taken at 24 and 36 h were denoted as early phase and late phase, respectively. NC indicates the phloroglucinol production strain harboring plasmid pCS-P$_{lpp1.0}$-HpdR-P$_{LlacO1}$-phlD. All data are reported as mean $\pm$ standard deviation from three biologically independent experiments ($n = 3$). All error bars represent standard deviation.

fermentation, phloroglucinol concentrations are approaching the peaks, while acetate concentrations approaching the bottom. At this time point, we predicted that cells would have undergone regulations, resulting in an optimized redox ratio. Therefore, we took samples at the two time points and measured the NADH/NAD$^+$ ratio. The results revealed that the groups subjected to bifunctional dynamic regulation had NADH/NAD$^+$ ratios comparable to the control group at 24-h. However, at 36-h, as fermentation progressed, the NADH/NAD$^+$ ratio of the negative control was significantly higher than that of the bifunctional regulation strains (Figure 6d). Specifically, during the late phase, the NADH/NAD$^+$ ratio of the negative control was at a level of 1.79-fold compared to the dynamic ndh-maeB group and 2.36-fold compared to the dynamic ndh-icd group. While the static control groups showed comparable NADH/NAD$^+$ ratios to the dynamic groups, the dynamic regulation contributed to even higher titer. This may be attributed to the constant regulation imposing excessive metabolic pressure on the cells. These results are consistent with our hypothesis, indicating that due to the integration of dynamic circuits, excess NADH was converted to NAD$^+$, and the redox pressure had been relieved for improving the carbon reallocation, diverting more carbon flux into acetyl-CoA downstream products.

4 | Discussion

Acetate overflow is a common challenge encountered in various microbial production pathways, and numerous metabolic engineering strategies have been designed to address this issue. However, achieving the desired results is often hindered by the intricate connections between acetate and cellular metabolism. In the current study, we developed an artificial dynamic regulation strategy to control overflow metabolism. By employing an acetate-responsive biosensor system, we successfully inhibited and overexpressed the NADH-related enzymes dynamically. Thus, the cellular redox ratio was modulated by following the dynamics of acetate accumulation, and the increased production of phloroglucinol demonstrated the enhanced supply of malonyl-CoA flow and improved carbon flux allocation. In addition to these direct effects, alterations in NADH levels may have widespread impacts on cellular metabolism. As the NADH/NAD$^+$ ratio primarily determines the redox state of cells, the changes could influence hundreds of cellular reactions (Berríos-Rivera 2002). Therefore, further investigation is needed to elucidate more detailed changes in the metabolome repertoire.

The phenomenon of acetate overflow reflects the occurrence of several metabolic events, including the production rate of acetyl-CoA exceeding its consumption rate, the glucose uptake rate surpassing the capacity of respiration, and the generation of NADH exceeding the oxidative capacity. Accordingly, we chose acetate as the effector for dynamic regulation to ensure the regulation is precisely applied when the metabolic issues arise. Inspired by this design, it is possible to choose different indicators for regulations in different contexts. For instance, ethanol could be a potential overflow indicator in yeast systems. In our study, we targeted genes encoding enzymes involved in NAD(P)H production within

the TCA cycle for inhibition. The production of phloroglucinol may benefit from the synergistic effects of reducing force decrease and the attenuation of the TCA cycle.

Acetate is not merely a wasteful byproduct of glycolysis; it also serves to adjust various metabolic processes within the cells. Indeed, acetate triggers changes in the expression levels of numerous genes in central metabolic pathways (Millard et al. 2021; Rau et al. 2016), indicating the presence of a complex self-regulatory network that responds to acetate and coordinate cell metabolism through various feedback mechanisms. However, the self-regulation of cells may tend to be mild, which could limit its effectiveness in achieving optimal regulatory outcomes in specific situations, such as fermentation. Surprisingly, by referring to a previous study (Millard et al. 2021), we noticed that most of the TCA genes we inhibited are included in the repertoire of genes whose expression is decreased in response to increased acetate concentration. Based on this observation, we speculated that through artificial intervention, we have augmented the cells' intrinsic regulatory mechanism, enabling cells to achieve more rapid and optimal regulatory in the fermentation scenario.

Moreover, the acetate-responsive regulation platform is available for further fine-tuning. Traditional engineering strategies, including promoter engineering, RBS engineering, regulator protein evolution, and configuration improvements, can be applied to tailor the biosensor system to acquire different regulatory profiles (Jiang et al. 2022). In addition, the CRISPRi system provides another avenue for engineering flexibility. By adjusting the sgRNA spacers, a variety of repression profiles can be achieved (Wang et al. 2021). This means that the regulatory network is highly flexible, and different regulatory profiles can be chosen for different production pathways. For example, to assist pathways that consume or produce reducing power, the regulation profile can be fine-tuned to achieve the desired redox ratio. In summary, this study provides a novel approach for exploiting metabolic byproducts to address acetate overflow, regulate central metabolism and balance cellular redox ratio, paving a way for the study of dynamic regulation-aided microbial production.

Author Contributions

J.Z., J.W. and Y.Y. conceived the idea. J.Z. designed and performed the experiments, analyzed the data, and wrote the manuscript. J.W., T.J., X.G., Q.G., Y.T., Y.Z., and A.D. participated the research. J.Z., J.W., T.J., X.G., Q.G., Y.T., Y.Z., A.D., and Y.Y. revised the manuscript. Y.Y. directed the research.

Conflicts of Interest

The authors declare no conflicts of interest.

Data Availability Statement

The data that support the findings of this study are available from the corresponding author upon reasonable request.

References

Abdel-Hamid, A. M., M. M. Attwood, and J. R. Guest. 2001. "Pyruvate Oxidase Contributes to the Aerobic Growth Efficiency of *Escherichia coli*." *Microbiology* 147: 1483–1498. https://doi.org/10.1099/00221287-147-6-1483.

Achkar, J., M. Xian, H. Zhao, and J. W. Frost. 2005. "Biosynthesis of Phloroglucinol." *Journal of the American Chemical Society* 127, no. 15: 5332–5333. https://doi.org/10.1021/ja042340g.

De Anda, R., A. R. Lara, V. Hernández, et al. 2006. "Replacement of the Glucose Phosphotransferase Transport System by Galactose Permease Reduces Acetate Accumulation and Improves Process Performance of *Escherichia coli* for Recombinant Protein Production Without Impairment of Growth Rate." *Metabolic Engineering* 8, no. 3: 281–290. https://doi.org/10.1016/j.ymben.2006.01.002.

Aristidou, A. A., K. Y. San, and G. N. Bennett. 1995. "Metabolic Engineering of Escherichia-Coli to Enhance Recombinant Protein-Production Through Acetate Reduction." *Biotechnology Progress* 11, no. 4: 475–478. https://doi.org/10.1021/bp00034a019.

Basan, M., S. Hui, H. Okano, et al. 2015. "Overflow Metabolism in *Escherichia coli* Results From Efficient Proteome Allocation." *Nature* 528, no. 7580: 99–104. https://doi.org/10.1038/nature15765.

Bauer, K. A., A. Benbassat, M. Dawson, V. T. Delapuente, and J. O. Neway. 1990. "Improved Expression of Human Interleukin-2 in High-Cell-Density Fermentor Cultures of *Escherichia coli* K-12 by a Phosphotransacetylase Mutant." *Applied and Environmental Microbiology* 56, no. 5: 1296–1302. https://doi.org/10.1128/Aem.56.5.1296-1302.1990.

Berríos-Rivera, S. 2002. "The Effect of Increasing NADH Availability on the Redistribution of Metabolic Fluxes in *Escherichia coli* Chemostat Cultures." *Metabolic Engineering* 4, no. 3: 230–237. https://doi.org/10.1006/mben.2002.0228.

Causey, T. B., K. T. Shanmugam, L. P. Yomano, and L. O. Ingram. 2004. "Engineering *Escherichia coli* for Efficient Conversion of Glucose to Pyruvate." *Proceedings of the National Academy of Sciences* 101, no. 8: 2235–2240. https://doi.org/10.1073/pnas.0308171100.

Contiero, J., C. Beatty, S. Kumari, C. L. DeSanti, W. R. Strohl, and A. Wolfe. 2000. "Effects of Mutations in Acetate Metabolism on High-Cell-Density Growth of *Escherichia coli*." *Journal of Industrial Microbiology & Biotechnology* 24, no. 6: 421–430. https://doi.org/10.1038/sj.jim.7000014.

Crabtree, H. G. 1929. "Observations on the Carbohydrate Metabolism of Tumours." *Biochemical Journal* 23, no. 3: 536–545. https://doi.org/10.1042/bj0230536.

d'Oelsnitz, S., W. Kim, N. T. Burkholder, et al. 2022. "Using Fungible Biosensors to Evolve Improved Alkaloid Biosyntheses." *Nature Chemical Biology* 18, no. 9: 981–989. https://doi.org/10.1038/s41589-022-01072-w.

Eiteman, M. A., and E. Altman. 2006. "Overcoming Acetate in *Escherichia coli* Recombinant Protein Fermentations." *Trends in Biotechnology* 24, no. 11: 530–536. https://doi.org/10.1016/j.tibtech.2006.09.001.

Enjalbert, B., P. Millard, M. Dinclaux, J. C. Portais, and F. Létisse. 2017. "Acetate Fluxes in *Escherichia coli* Are Determined by the Thermodynamic Control of the Pta-AckA Pathway." *Scientific Reports* 7: 42135. https://doi.org/10.1038/srep42135.

Farmer, W. R., and J. C. Liao. 2000. "Improving Lycopene Production in *Escherichia coli* by Engineering Metabolic Control." *Nature Biotechnology* 18, no. 5: 533–537. https://doi.org/10.1038/75398.

Gecse, G., R. Labunskaite, M. Pedersen, M. Kilstrup, and T. Johanson. 2024. "Minimizing Acetate Formation From Overflow Metabolism in *Escherichia coli*: Comparison of Genetic Engineering Strategies to Improve Robustness Toward Sugar Gradients in Large-Scale Fermentation Processes." *Frontiers in Bioengineering and Biotechnology* 12: 1339054. https://doi.org/10.3389/fbioe.2024.1339054.

Gibson, D. G., L. Young, R. Y. Chuang, J. C. Venter, C. A. Hutchison, and H. O. Smith. 2009. "Enzymatic Assembly of DNA Molecules up to Several Hundred Kilobases." *Nature Methods* 6, no. 5: 343-U341. https://doi.org/10.1038/Nmeth.1318.

Gray, D. A., G. Dugar, P. Gamba, H. Strahl, M. J. Jonker, and L. W. Hamoen. 2019. "Extreme Slow Growth as Alternative Strategy to Survive Deep Starvation in Bacteria." *Nature Communications* 10, no. 1: 890. https://doi.org/10.1038/s41467-019-08719-8.

Gupta, A., I. M. B. Reizman, C. R. Reisch, and K. L. J. Prather. 2017. "Dynamic Regulation of Metabolic Flux in Engineered Bacteria Using a Pathway-Independent Quorum-Sensing Circuit." *Nature Biotechnology* 35, no. 3: 273–279. https://doi.org/10.1038/nbt.3796.

Hanko, E. K. R., N. P. Minton, and N. Malys. 2017. "Characterisation of a 3-Hydroxypropionic Acid-Inducible System From Pseudomonas Putida for Orthogonal Gene Expression Control in *Escherichia coli* and Cupriavidus Necator." *Scientific Reports* 7: 1724. https://doi.org/10.1038/s41598-017-01850-w.

Harden, A. 1901. "LXIV.—The Chemical Action of Bacillus Coli Communis and Similar Organisms on Carbohydrates and Allied Compounds." *Journal of the Chemical Society, Transactions* 79: 610–628. https://doi.org/10.1039/ct9017900610.

Heux, S., R. Cachon, and S. Dequin. 2006. "Cofactor Engineering In *Saccharomyces cerevisiae*: Expression of a H_2O-forming NADH Oxidase and Impact on Redox Metabolism." *Metabolic Engineering* 8, no. 4: 303–314. https://doi.org/10.1016/j.ymben.2005.12.003.

Holm, A. K., L. M. Blank, M. Oldiges, et al. 2010. "Metabolic and Transcriptional Response to Cofactor Perturbations in *Escherichia coli*." *Journal of Biological Chemistry* 285, no. 23: 17498–17506. https://doi.org/10.1074/jbc.M109.095570.

Jensen, E. B., and S. Carlsen. 1990. "Production of Recombinant Human Growth-Hormone in Escherichia-Coli—Expression of Different Precursors and Physiological-Effects of Glucose, Acetate, and Salts." *Biotechnology and Bioengineering* 36, no. 1: 1–11. https://doi.org/10.1002/bit.260360102.

Jiang, T., C. Li, Y. Zou, J. Zhang, Q. Gan, and Y. Yan. 2022. "Establishing an Autonomous Cascaded Artificial Dynamic (AutoCAD) Regulation System for Improved Pathway Performance." *Metabolic Engineering* 74: 1–10. https://doi.org/10.1016/j.ymben.2022.08.009.

Khan, F., N. Tabassum, N. I. Bamunuarachchi, and Y. M. Kim. 2022. "Phloroglucinol and Its Derivatives: Antimicrobial Properties Toward Microbial Pathogens." *Journal of Agricultural and Food Chemistry* 70, no. 16: 4817–4838. https://doi.org/10.1021/acs.jafc.2c00532.

Kim, M. M., and S. K. Kim. 2010. "Effect of Phloroglucinol on Oxidative Stress and Inflammation." *Food and Chemical Toxicology* 48, no. 10: 2925–2933. https://doi.org/10.1016/j.fct.2010.07.029.

Koh, B. T., U. Nakashimada, M. Pfeiffer, and M. G. S. Yap. 1992. "Comparison of Acetate Inhibition on Growth of Host and Recombinante. Coli K12 Strains." *Biotechnology Letters* 14, no. 12: 1115–1118. https://doi.org/10.1007/Bf01027012.

Li, C., Y. Zhou, Y. Zou, T. Jiang, X. Gong, and Y. Yan. 2023. "Identifying, Characterizing, and Engineering a Phenolic Acid-Responsive Transcriptional Factor From." *ACS Synthetic Biology* 12, no. 8: 2382–2392. https://doi.org/10.1021/acssynbio.3c00206.

Liu, Y., R. Landick, and S. Raman. 2019. "A Regulatory NADH/NAD+ Redox Biosensor for Bacteria." *ACS Synthetic Biology* 8, no. 2: 264–273. https://doi.org/10.1021/acssynbio.8b00485.

Maddocks, S. E., and P. C. F. Oyston. 2008. "Structure and Function of the LysR-Type Transcriptional Regulator (LTTR) Family Proteins." *Microbiology* 154: 3609–3623. https://doi.org/10.1099/mic.0.2008/022772-0.

March, J. C., M. A. Eiteman, and E. Altman. 2002. "Expression of an Anaplerotic Enzyme, Pyruvate Carboxylase, Improves Recombinant Protein Production In." *Applied and Environmental Microbiology* 68, no. 11: 5620–5624. https://doi.org/10.1128/Aem.68.11.5620-5624.2002.

De Mey, M., S. De Maeseneire, W. Soetaert, and E. Vandamme. 2007. "Minimizing Acetate Formation in *E. coli* Fermentations." *Journal of Industrial Microbiology & Biotechnology* 34, no. 11: 689–700. https://doi.org/10.1007/s10295-007-0244-2.

Millard, P., B. Enjalbert, S. Uttenweiler-Joseph, J. C. Portais, and F. Létisse. 2021. "Control and Regulation of Acetate Overflow in *Escherichia coli*." *eLife* 10: e63661. https://doi.org/10.7554/eLife.63661.

Millard, P., T. Gosselin-Monplaisir, S. Uttenweiler-Joseph, and B. Enjalbert. 2023. "Acetate Is a Beneficial Nutrient for *E. coli* at Low Glycolytic Flux." *EMBO Journal* 42, no. 15: e113079. https://doi.org/10.15252/embj.2022113079.

Nakano, K., M. Rischke, S. Sato, and H. Märkl. 1997. "Influence of Acetic Acid on the Growth of *Escherichia coli* K12 During High-Cell-Density Cultivation in a Dialysis Reactor." *Applied Microbiology and Biotechnology* 48, no. 5: 597–601. https://doi.org/10.1007/s002530051101.

Parenteau, J., L. Maignon, M. Berthoumieux, M. Catala, V. Gagnon, and S. Abou Elela. 2019. "Introns Are Mediators of Cell Response to Starvation." *Nature* 565, no. 7741: 612–617. https://doi.org/10.1038/s41586-018-0859-7.

Rau, M. H., P. Calero, R. M. Lennen, K. S. Long, and A. T. Nielsen. 2016. "Genome-Wide *Escherichia coli* Stress Response and Improved Tolerance Towards Industrially Relevant Chemicals." *Microbial Cell Factories* 15: 176. https://doi.org/10.1186/s12934-016-0577-5.

Rogers, J. K., and G. M. Church. 2016. "Genetically Encoded Sensors Enable Real-Time Observation of Metabolite Production." *Proceedings of the National Academy of Sciences* 113, no. 9: 2388–2393. https://doi.org/10.1073/pnas.1600375113.

Teng, Y., J. Zhang, T. Jiang, Y. Zou, X. Gong, and Y. Yan. 2022. "Biosensor-Enabled Pathway Optimization in Metabolic Engineering." *Current Opinion in Biotechnology* 75: 102696. https://doi.org/10.1016/j.copbio.2022.102696.

Thomason, L. C., N. Costantino, and D. L. Court. 2007. "*E. coli* Genome Manipulation by P1 Transduction." *Current Protocols in Molecular Biology* 79, no. 1: 1–8. https://doi.org/10.1002/0471142727.mb0117s79.

Tran, Q. H., J. Bongaerts, D. Vlad, and G. Unden. 1997. "Requirement for the Proton-Pumping Nadh Dehydrogenase I of *Escherichia coli* in Respiration of NADH to Fumarate and Its Bioenergetic Implications." *European Journal of Biochemistry* 244, no. 1: 155–160. https://doi.org/10.1111/j.1432-1033.1997.00155.x.

Vadali, R. 2004. "Cofactor Engineering of Intracellular CoA/Acetyl-Coa and Its Effect on Metabolic Flux Redistribution in *Escherichia coli*." *Metabolic Engineering* 6, no. 2: 133–139. https://doi.org/10.1016/j.ymben.2004.02.001.

Vemuri, G. N., E. Altman, D. P. Sangurdekar, A. B. Khodursky, and M. A. Eiteman. 2006. "Overflow Metabolism in *Escherichia coli* During Steady-State Growth: Transcriptional Regulation and Effect of the Redox Ratio." *Applied and Environmental Microbiology* 72, no. 5: 3653–3661. https://doi.org/10.1128/AEM.72.5.3653-3661.2006.

Vemuri, G. N., M. A. Eiteman, and E. Altman. 2006. "Increased Recombinant Protein Production Inescherichia Colistrains With Overexpressed Water-Forming NADH Oxidase and a Deleted ArcA Regulatory Protein." *Biotechnology and Bioengineering* 94, no. 3: 538–542. https://doi.org/10.1002/bit.20853.

Vemuri, G. N., M. A. Eiteman, J. E. McEwen, L. Olsson, and J. Nielsen. 2007. "Increasing NADH Oxidation Reduces Overflow Metabolism in." *Proceedings of the National Academy of Sciences* 104, no. 7: 2402–2407. https://doi.org/10.1073/pnas.0607469104.

Wang, J., C. Li, T. Jiang, and Y. Yan. 2023. "Biosensor-Assisted Titratable CRISPRi High-Throughput (BATCH) Screening for Over-Production Phenotypes." *Metabolic Engineering* 75: 58–67. https://doi.org/10.1016/j.ymben.2022.11.004.

Wang, J., R. Zhang, J. Zhang, et al. 2021. "Tunable Hybrid Carbon Metabolism Coordination for the Carbon-Efficient Biosynthesis of 1,3-Butanediol in." *Green Chemistry* 23, no. 21: 8694–8706. https://doi.org/10.1039/d1gc02867g.

Warburg, O. 1956. "On Respiratory Impairment in Cancer Cells." *Science* 124, no. 3215: 269–270. https://www.ncbi.nlm.nih.gov/pubmed/13351639.

Wong, M. S., S. Wu, T. B. Causey, G. N. Bennett, and K. Y. San. 2008. "Reduction of Acetate Accumulation in *Escherichia coli* Cultures for Increased Recombinant Protein Production." *Metabolic Engineering* 10, no. 2: 97–108. https://doi.org/10.1016/j.ymben.2007.10.003.

Yang, Y. T., G. N. Bennett, and K. Y. San. 1999. "Effect of Inactivation of Nuo and ackA-pta on Redistribution of Metabolic Fluxes in *Escherichia coli*." *Biotechnology and Bioengineering* 65, no. 3: 291–297. https://www.ncbi.nlm.nih.gov/pubmed/10486127.

Yu, S., L. Guo, L. Zhao, Z. Chen, and Y. Huo. 2020. "Metabolic Engineering of *E. coli* for Producing Phloroglucinol From Acetate." *Applied Microbiology and Biotechnology* 104, no. 18: 7787–7799. https://doi.org/10.1007/s00253-020-10591-2.

Zha, W., S. B. Rubin-Pitel, and H. Zhao. 2006. "Characterization of the Substrate Specificity of PhlD, a Type III Polyketide Synthase From." *Journal of Biological Chemistry* 281, no. 42: 32036–32047. https://doi.org/10.1074/jbc.M606500200.

Zhang, F., J. M. Carothers, and J. D. Keasling. 2012. "Design of a Dynamic Sensor-Regulator System for Production of Chemicals and Fuels Derived From Fatty Acids." *Nature Biotechnology* 30, no. 4: 354–359. https://doi.org/10.1038/nbt.2149.

Zhang, G. C., J. J. Liu, and W. T. Ding. 2012. "Decreased Xylitol Formation During Xylose Fermentation in *Saccharomyces cerevisiae* Due to Overexpression of Water-Forming NADH Oxidase." *Applied and Environmental Microbiology* 78, no. 4: 1081–1086. https://doi.org/10.1128/Aem.06635-11.

Zou, Y., J. Zhang, J. Wang, X. Gong, T. Jiang, and Y. Yan. 2024. "A Self-Regulated Network for Dynamically Balancing Multiple Precursors in Complex Biosynthetic Pathways." *Metabolic Engineering* 82: 69–78. https://doi.org/10.1016/j.ymben.2024.02.001.

Supporting Information

Additional supporting information can be found online in the Supporting Information section.